

1 High-level cognition is supported by information-rich but
2 compressible brain activity patterns

3 Lucy L. W. Owen^{1,2} and Jeremy R. Manning^{1,*}

1¹Department of Psychological and Brain Sciences,
Dartmouth College, Hanover, NH

²Carney Institute for Brain Sciences,
Brown University, Providence, RI

*Address correspondence to jeremy.r.manning@dartmouth.edu

4 December 26, 2023

5 **Abstract**

6 We Brain activity patterns are highly flexible and often complex, but also highly structured.
7 Here we examined how fundamental properties of brain activity patterns relate to ongoing
8 cognitive processes. To this end, we applied dimensionality reduction algorithms and pattern
9 classifiers to functional neuroimaging data collected as participants listened to a story, tem-
10 porally scrambled versions of the story, or underwent a resting state scanning session. These
11 experimental conditions were intended to require different depths of processing and inspire
12 different levels of cognitive engagement. We considered two primary aspects of the data. First,
13 we treated the maximum achievable decoding accuracy across participants as an indicator of
14 the “informativeness” of the recorded patterns. Second, we treated the number of features
15 (components) required to achieve a threshold decoding accuracy as a proxy for the “compress-
16 ibility” of the neural patterns (where fewer components indicate greater compression). Overall,
17 we found that the peak decoding accuracy (achievable without restricting the numbers of fea-
18 tures) was highest in the intact (unscrambled) story listening condition. However, the number
19 of features required to achieve comparable classification accuracy was also lowest in the intact
20 story listening condition. Taken together, our work suggests that our brain networks flexibly
21 reconfigure according to ongoing task demands, and that the activity patterns associated with
22 higher-order cognition and high engagement are both more informative and more compressible
23 than the activity patterns associated with lower-order tasks and lower levels of engagement.

24 **Keywords:** information, compression, temporal decoding, dimensionality reduction, neu-
25 roimaging

26 **Significance Statement:** How our brains respond to ongoing experiences depends on what
27 we are doing and thinking about, among other factors. To study how brain activity reflects
28 ongoing cognition, we examined two fundamental aspects of brain activity under different
29 cognitive circumstances: informativeness and compressibility. Informativeness refers to the
30 extent to which brain patterns are both temporally specific and consistent across different
31 people. Compressibility refers to how robust the informativeness of brain patterns is to
32 dimensionality reduction. Brain activity evoked by higher-level cognitive tasks are both more
33 informative and more compressible than activity evoked by lower-level tasks. Our findings
34 suggest that our brains flexibly reconfigure themselves to optimize different aspects of how
35 they function according to ongoing cognitive demands.

36 Introduction

37 Large-scale networks, including the human brain, may be conceptualized as occupying one or
38 more positions along on a continuum. At one extreme, every node is fully independent from
39 every other node. At the other extreme, all nodes behave identically. Each extreme optimizes
40 key properties of how the network functions. When every node is independent, the network is
41 maximally *expressive*: if we define the network's "state" as the activity pattern across its nodes,
42 then every state is equally reachable by a network with fully independent nodes. On the other
43 hand, a network of identically behaved nodes optimizes *robustness*: any subset of nodes may
44 be removed from the network without any loss of function or expressive power, as long as any
45 single node remains. In addition to considering flexibility across space (nodes), these properties
46 may also vary largely independently across time. A network is maximally expressive when
47 its nodes' activity patterns vary in meaningful ways from moment to moment, whereas it is
48 maximally robust to signal corruption when its activity is constant over time. Presumably, most
49 natural systems tend to occupy positions between these extremes. temporal and spatial extremes.
50 Under different circumstances, it may even prove beneficial for systems to make different tradeoffs
51 between expressiveness and robustness along the temporal and spatial dimensions. We wondered:
52 might the human brain reconfigure itself to be more flexible or more robust according to ongoing
53 demands? In other words, might the brain reconfigure its connections or behaviors under different
54 circumstances to change its position along this continuumthese continuums?

55 Closely related to the above notions of expressiveness versus robustness are measures of
56 how much *information* is contained in a given signal or pattern, and how *redundant* a signal
57 is (Shannon, 1948). Formally, information is defined as the amount of uncertainty about a given
58 variables' outcomes (i.e., entropy), measured in *bits*, or the optimal number of yes/no questions
59 needed to reduce uncertainty about the variable's outcomes to zero. Highly complex systems with
60 many degrees of freedom (i.e., high flexibility and expressiveness), are more information-rich than
61 simpler or more constrained systems. The redundancy of a signal denotes the difference between
62 how expressive the signal *could* be (i.e., proportional to the number of unique states or symbols
63 used to transmit the signal) and the actual information rate (i.e., the entropy of each individual
64 state or symbol). If a brain network's nodes are fully independent, then the number of bits required

65 to express a single activity pattern is proportional to the number of nodes. The network would
66 also be minimally redundant, since the status of every node would be needed to fully express a
67 single brain activity pattern. If a brain network's nodes are fully coupled and identical, then the
68 number of bits required to express a single activity pattern is proportional to the number of unique
69 states or values any individual node can take on. Such a network would be highly redundant,
70 since knowing any individual node's state would be sufficient to recover the full-brain activity
71 pattern. Highly redundant systems are also robust, since there is little total information loss due
72 to removing any given observation.

73 We take as a given that brain activity is highly flexible: our brains can exhibit nearly infinite
74 varieties of activity patterns. This flexibility implies that our brains' activity patterns are highly
75 information rich. However, brain activity patterns are also highly structured. For example,
76 full-brain correlation matrices are stable within (Finn et al., 2017, 2015; Gratton et al., 2018) and
77 across (Cole et al., 2014; Glerean et al., 2012; Gratton et al., 2018; Yeo et al., 2011) individuals. This
78 stability suggests that our brains' activity patterns are at least partially constrained, for example
79 by anatomical, external, or internal factors. Constraints on brain activity that limit its flexibility
80 decrease expressiveness (i.e., its information rate). However, constraints on brain activity also
81 increase its robustness to noise (e.g., "missing" or corrupted signals may be partially recovered).
82 For example, recent work has shown that full-brain activity patterns may be reliably recovered
83 from only a relatively small number of implanted electrodes (Owen et al., 2020; Scangos et al.,
84 2021). This robustness property suggests that the relevant signal (e.g., underlying factors that
85 have some influence over brain activity patterns) are compressible.

86 To the extent that brain activity patterns contain rich task-relevant information, we should be
87 able to use the activity patterns to accurately differentiate between different aspects of a task (e.g.,
88 using pattern classifiers; Norman et al., 2006). For example, prior work has shown a direct
89 correspondence between classification accuracy and the information content of a signal (Alvarez,
90 2002). To the extent that brain activity patterns are compressible, we should be able to generate
91 simplified (e.g., lower dimensional) representations of the data while still preserving the relevant
92 or important aspects of the original signal. In general, information content and compressibility
93 are often related but are partially also dissociable (Fig. 1). If a given signal (e.g., a representation
94 of brain activity patterns) contains more information about ongoing cognitive processes, then the

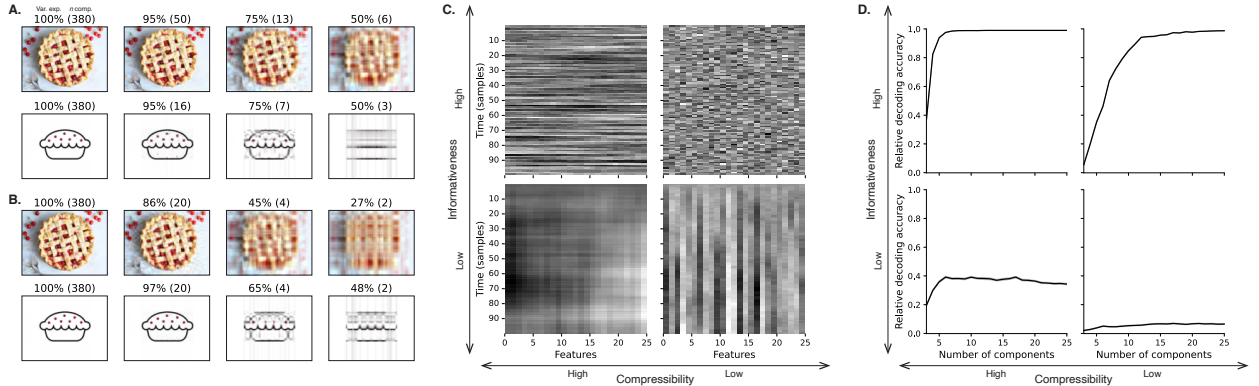


Figure 1: Information content and compressibility. **A. Variance explained for two images.** Consider two example images: a photograph and simple drawing. The images have the same resolutions, but their content is very different. The photograph is more information rich: when we compare the original photograph and drawing (leftmost column), we can see that the photograph captures much more detail. We applied principal components analysis to a photograph and drawing the images, treating the rows of the images as “observations.” Across columns, we identified the numbers of components required to explain 100%, 95%, 75%, or 50% of the cumulative variance in each image (the 100% columns denote the original images). The numbers of components are indicated in parentheses, and the resulting “compressed” images are displayed. This analysis reveals that the drawing is more compressible: just 16 components can explain 95% of the variance in the drawing, whereas 50 components are required to explain 95% of the variance in the photograph. **B. Representing two images with different numbers of components.** Using the same principal component decompositions as in Panel A, we computed the cumulative proportion of variance explained with 380 (original images), 20, 4, or 2 components. **C. Cumulative variance explained versus number of components.** For the images displayed in Panels A and B, we plot the cumulative proportion of variance explained as a function of the number of components used to represent each image. **D. Information rate and compressibility.** Across multiple images, by showing that the information rate (i.e., the amount of information contained in the same number of components) can explain more variance in the drawing than in the photograph. **C. Template data from four synthetic datasets.** We constructed four synthetic datasets, each image comprising 25 features (columns) and 100 samples (rows). The datasets were simulated to contain different levels of informativeness and compressibility (see Synthetic data). Compressibility is related to the number of participants. High-information-rate images tend to be high-resolution, contain different levels of informativeness, and low-information-rate images tend to be low-resolution. **D. Decoding accuracy by number of components.** For each synthetic dataset, we trained across-participant classifiers to decode timepoint labels. Each panel displays the difference between decoding accuracy as a function of the information required to specify the original versus compressed images (vertical axis). Highly compressible images often contain predictable structure (redundancies) that can be leveraged to represent the images much more efficiently than in their original feature spaces. Error ribbons denote bootstrap-estimated 95% confidence intervals.

95 peak decoding accuracy should be high. ~~And if the~~ In the simulations shown in Figure 1C we
96 construct synthetic datasets that have high or low levels of informativeness by varying temporal
97 autocorrelations in the data (see *Synthetic data*). If a signal is compressible, then a low-dimensional
98 embedding of the signal will be similarly informative as the original signal. In the simulations
99 shown in Figure 1C we construct synthetic datasets that have high or low levels of compressibility
100 by varying the covariance structure across features (see *Synthetic data*). As shown in Figure 1D,
101 highly informative datasets yield higher decoding accuracies than less informative datasets (i.e.,
102 the peaks of the curves in the top panels of Fig. 1D) are higher than the peaks of the curves in
103 the bottom panels). Highly compressible datasets show steeper slopes when we plot decoding
104 accuracy as a function of the number of components used to represent the data (i.e., the slopes
105 of the curves in the left panels of Fig. 1D are steeper than the slopes of the curves in the right
106 panels). Whereas characterizing the informativeness and compressibility of synthetic data can
107 be instructive, we are ultimately interested in understanding how these properties relate to brain
108 activity patterns recorded under different cognitive circumstances.

109 Several recent studies suggest that the complexity of brain activity is task-dependent, whereby
110 simpler tasks with lower cognitive demands are reflected by simpler and more compressible brain
111 activity patterns, and more complex tasks with higher cognitive demands are reflected by more
112 complex and less compressible brain activity patterns (Mack et al., 2020; Owen et al., 2021). These
113 patterns hold even when the stimulus itself is held constant (Mack et al., 2020). These findings
114 complement other work suggesting that functional connectivity (correlation) patterns are task-
115 dependent (Cole et al., 2014; Finn et al., 2017; Owen et al., 2020), although see Gratton et al. (2018).
116 Higher-order cognitive processing of a common stimulus also appears to drive more stereotyped
117 task-related activity and functional connectivity across individuals (Hasson et al., 2008; Lerner et
118 al., 2011; Simony & Chang, 2020; Simony et al., 2016).

119 The above studies are consistent with two potential descriptions of how cognitive processes
120 are reflected in brain activity patterns. One possibility is that the information rate of brain activity
121 increases during more complex or higher-level cognitive processing. If so, then the ability to
122 reliably decode cognitive states from brain activity patterns should improve with task complexity
123 or with the level (or “depth”) of cognitive processing. A second possibility is that the compress-
124 ability of brain activity patterns ~~increases decreases~~ during more complex or higher-level cognitive

125 processing. If so, then individual features of brain recordings ~~, or compressed representations of~~
126 ~~brain recordings,~~ should carry more information (over and above the information carried by other
127 features) during complex or high-level (versus simple or low-level) cognitive tasks. The tradeoffs
128 between these two aspects of brain activity may also vary across brain regions or networks, for
129 example according to each region's functional role.

130 We used a previously collected neuroimaging dataset to estimate the extent to which each of
131 these two possibilities might hold. The dataset we examined comprised functional magnetic reso-
132 nance imaging (fMRI) data collected as participants listened to an audio recording of a ~~10-minute~~
133 7-minute story, temporally scrambled recordings of the story, or underwent a resting state scan (Si-
134 mony et al., 2016). Each of these experimental conditions evokes different depths of cognitive
135 processing (Hasson et al., 2008; Lerner et al., 2011; Owen et al., 2021; Simony et al., 2016). We used
136 across-participant classifiers to decode listening times in each condition, as a proxy for how "infor-
137 mative" the task-specific activity patterns were (Simony & Chang, 2020). We also used principle
138 components analysis to generate lower-dimensional representations of the activity patterns. We
139 then repeated the classification analyses after preserving different numbers of components and
140 examined how classification accuracy changed across the different experimental conditions.

141 Results

142 We sought to understand whether higher-level cognition is reflected by more reliable and in-
143 formative brain activity patterns, and how compressibility of brain activity patterns relates to
144 cognitive complexity. We developed a computational framework for systematically assessing the
145 informativeness and compressibility of brain activity patterns recorded under different cognitive
146 circumstances. We used across-participant decoding accuracy (see *Forward inference and decoding*
147 *accuracy*) as a proxy for informativeness. To estimate the compressibility of the brain patterns, we
148 used group principal components analysis (PCA) to project the brain patterns into k -dimensional
149 spaces, for different values of k (see *Hierarchical Topographic Factor Analysis (HTFA)* and *Principal*
150 *components analysis (PCA)*). For more compressible brain patterns, decoding accuracy should be
151 more robust to small values of k .

152 We analyzed a dataset collected by Simony et al. (2016) that comprised four experimental

153 conditions. These conditions exposed participants to stimuli that systematically varied in cognitive
154 engagement. In the *intact* experimental condition, participants listened to an audio recording
155 of a 10-minute~~7-minute~~ Moth Radio Hour story, *Pie Man*, by Jim O’Grady. In the *paragraph-*
156 *scrambled* experimental condition, participants listened to a temporally scrambled version of
157 the story, where the paragraphs occurred out of order, but where the same set of paragraphs
158 was presented over the entire listening interval. All participants in this condition experienced
159 the scrambled paragraphs in the same order. In the *word*-scrambled experimental condition,
160 participants listened to a temporally scrambled version of the story, where the words occurred in
161 a random order. Again, all participants in this condition experienced the scrambled words in the
162 same order. Finally, in the *rest* experimental condition, participants lay in the scanner with no overt
163 stimulus, while keeping their eyes open and blinking as needed. This public dataset provided
164 a convenient means for testing our hypothesis that different levels of cognitive processing and
165 engagement affect how informative and compressible the associated brain patterns are.

166 To evaluate the relation between informativeness and compressibility for brain activity from
167 each experimental condition, we trained a series of across-participant temporal decoders on com-
168 pressed representations of the data. Figure 2A displays the decoding accuracy as a function
169 of the number of principal components used to represent the data (also see Fig. S1). Several
170 patterns were revealed by the analysis. First, in general (i.e., across experimental conditions),
171 decoding accuracy tends to improve as the number of components are increased. However, de-
172 coding accuracy peaked at higher levels for experimental conditions that exposed participants
173 to cognitively richer stimuli (Fig. 2D). The peak decoding accuracy was highest for the “in-
174 tact” condition (versus paragraph: $t(99) = 35.205, p < 0.001$) ~~$t(99) = 35.205, p < 0.001$~~ ; versus word:
175 ~~$t(99) = 43.172, p < 0.001$~~ $t(99) = 43.172, p < 0.001$; versus rest: $t(99) = 81.361, p < 0.001$ ~~$t(99) = 81.361, p < 0.001$~~ ,
176 next highest for the “paragraph” condition (versus word: $t(99) = 6.243, p < 0.001$) ~~$t(99) = 6.243, p < 0.001$~~ ;
177 versus rest: $t(99) = 50.748, p < 0.001$ ~~$t(99) = 50.748, p < 0.001$~~ , and next highest for the “word” con-
178 dition (versus rest: $t(99) = 48.791, p < 0.001$) ~~$t(99) = 48.791, p < 0.001$~~). This ordering implies that
179 cognitively richer conditions evoke more stable brain activity patterns across people.

180 The cognitively richer conditions also displayed steeper initial slopes. For example, the intact
181 condition decoders reached an arbitrarily chosen threshold of 5% accuracy using fewer components
182 than the paragraph condition decoders ($t(99) = -7.429, p < 0.001$) or word condition decoders

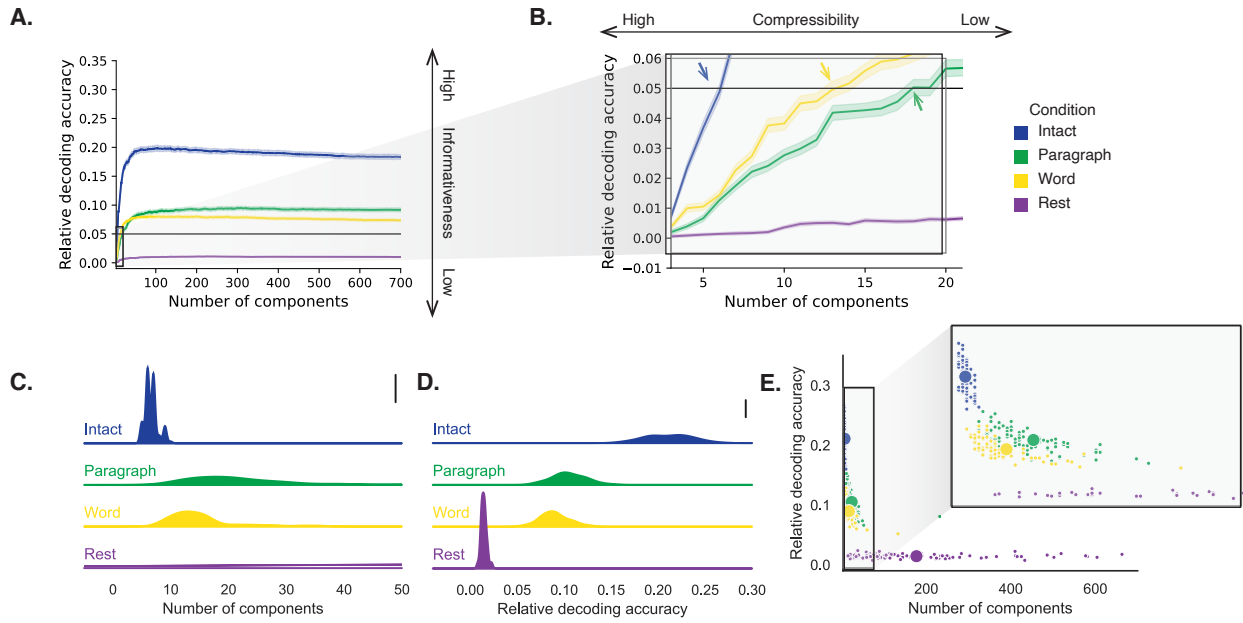


Figure 2: Decoding accuracy and compressibility.

A. Decoding accuracy by number of components. Ribbons of each color display cross-validated decoding performance for each condition (intact, paragraph, word, and rest), as a function of the number of components (features) used to represent the data. For each condition, decoding accuracy has been normalized by subtracting expected “chance” decoding performance (estimated as $\frac{1}{T}$, where T is the number of timepoints in the given condition). This normalization was intended to enable fairer comparisons across conditions; a relative decoding accuracy of 0.0 denotes “chance” performance. The horizontal black line denotes 5% decoding accuracy (used as a reference in Panel B).

B. Numbers of components required to reach a fixed decoding accuracy threshold, by condition. The panel displays a zoomed-in view of the inset in Panel A. Intersections between each condition’s decoding accuracy curve and the 5% decoding accuracy reference line are marked by arrows. All error ribbons in Panels A and B denote bootstrap-estimated 95% confidence intervals.

C. Estimating “compressibility” for each condition. The probability density plots display the numbers of components required to reach at least 5% (corrected) decoding accuracy, across all cross validation runs. For the “rest” condition, where decoding accuracy never reached 5% accuracy, we display the distribution of the numbers of components required to achieve the peak decoding accuracy in each fold. (This distribution is nearly flat, as also illustrated in Panel E.) The scale bar denotes a height of 0.01.

D. Estimating “informativeness” for each condition. The probability density plots display the peak (corrected) decoding accuracies achieved in each condition, across all cross validation runs. The scale bar denotes a height of 0.01.

E. Informativeness versus compressibility. Each dot displays the minimum number of components required to achieve at least 5% corrected decoding accuracy (x -coordinate; for the rest condition the numbers of components are estimated using the peak decoding accuracies as in Panel C) and the peak (corrected) decoding accuracy (y -coordinate). The smaller dots correspond to individual cross validation runs and the larger dots display the averages across runs. The inset displays a zoomed-in view of the indicated region in the main panel.

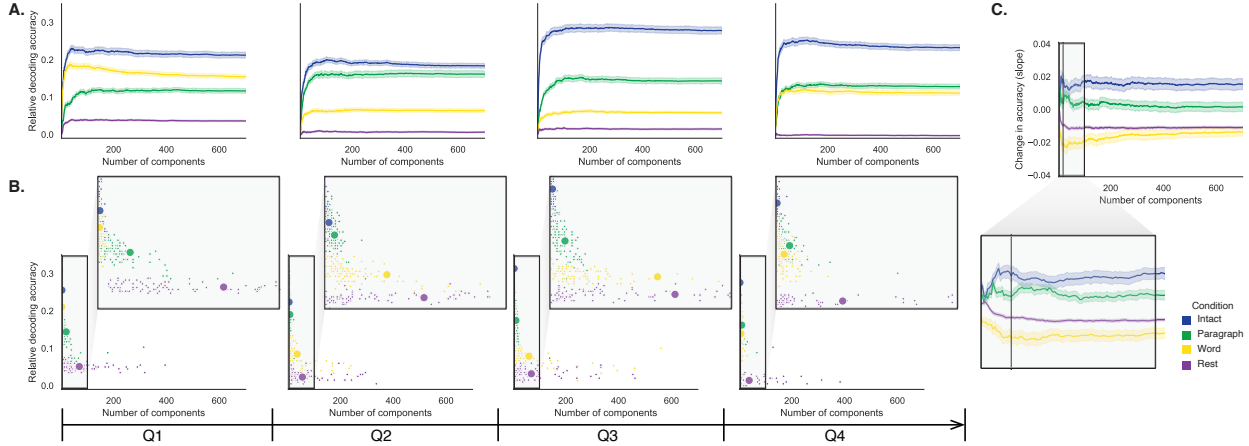


Figure 3: Changes in decoding accuracy and compression over time. **A. Decoding accuracy by number of components, by story segment.** Each family of curves is plotted in the same format as Figure 2A but reflects data only from one quarter of the dataset. **B. Informativeness versus compressibility by condition and segment.** Each scatter plot is in the same format as Figure 2E, but reflects data only from one quarter of the dataset. **C. Change in decoding accuracy over time, by number of components.** For each number of components (*x*-axis) and condition (color), we fit a regression line to the decoding accuracies obtained for the first, second, third, and fourth quarters of the dataset (corresponding to the columns of Panels A and B). The *y*-axis denotes the slopes of the regression lines. The black vertical line marks $k = 20$ components, as referenced in the main text. All error ribbons denote bootstrap-estimated 95% confidence intervals.

183 ($t(99) = -7.300, p < 0.001$), and decoding accuracy never exceeded 5% for the rest condition. This
 184 suggests that brain activity patterns evoked by cognitively richer conditions are more compressible,
 185 such that representing the data using the same number of principal components provides more
 186 information to the temporal decoders (Figs. 2B, C). Taken together, as shown in Figure 2E, we
 187 found that brain activity patterns evoked by cognitively richer conditions tended to be both more
 188 informative (i.e., associated with higher peak decoding accuracies) *and* more compressible (i.e.,
 189 requiring fewer components to achieve the 5% accuracy threshold).

190 If informativeness (to the temporal decoders) and compressibility vary with the cognitive
 191 richness of the stimulus, might these measures also vary over time *within* a given condition? For
 192 example, participants in the intact condition might process the ongoing story more deeply later
 193 on in the story (compared with earlier in the story) given the additional narrative background
 194 and context they had been exposed to by that point. To examine this possibility, we divided each
 195 condition into four successive time segments. We computed decoding curves (Fig. 3A) and the
 196 numbers of components required to achieve 5% decoding accuracy (Fig. 3B) for each segment and

197 condition. We found that, in the two most cognitively rich conditions (intact and paragraph), both
198 decoding accuracy and compressibility, as reflected by the change in decoding curves, increased
199 with listening time (e.g., at the annotated reference point of $k = 20$ components in Fig. 3C: intact:
200 $t(99) = 7.915, p < 0.001$; paragraph: $t(99) = 2.354, p = 0.021$). These changes may reflect an increase
201 in comprehension or depth of processing with listening time. In contrast, the decoding accuracy
202 and compressibility *decreased* with listening time in the word condition ($t(99) = -10.747, p < 0.001$)
203 and rest condition ($t(99) = -22.081, p < 0.001$). This might reflect the depletion of attentional
204 resources in the less-engaging word and rest conditions.

205 These results make some intuitive sense. As the contextual information available to participants
206 increases (i.e., over time in the cognitively rich intact and paragraph conditions), it makes sense that
207 this might constrain neural responses to a greater extent. While this pattern may not necessarily
208 hold for every possible story or stimulus, we suspect that it is generally the case that our knowledge
209 about what is happening in a story tends to increase as we experience more of it. In turn, this
210 could lead to greater consistency in different people's interpretations of and neural responses to
211 the stimulus. Similarly, as participants are left to "mind wander," or as they experience mental
212 fatigue (i.e., over time in the less cognitively rich word and rest conditions), we suggest that this
213 might lead to greater variability in neural responses across people, resulting in lower decoding
214 accuracy. Again, it is not necessarily the case that every possible "unengaging" stimulus will
215 lead to greater neural variability as time progresses, but we suspect this phenomenon is likely to
216 hold for a variety of such stimuli. These findings replicate at least to a limited extent (e.g., across
217 both cognitively rich conditions and across both cognitively impoverished conditions, and for the
218 different groups of participants in each of those conditions). However, determining whether these
219 patterns generalize to other stimuli would require additional study (with new stimuli).

220 We also wondered how If the informativeness and compressibility in the different experimental
221 conditions might of brain activity patterns vary over time, might these properties also vary across
222 brain networks—? We used a network parcellation identified by Yeo et al. (2011) to segment the
223 brain into seven distinct networks. The networks can be sorted (roughly) in order from lower-level
224 to higher-level cortex as follows (Figs. 4A–C): visual, somatomotor, dorsal attention, ventral atten-
225 tion, limbic, frontoparietal, and default mode. Next, we computed decoding curves separately for
226 the activity patterns within each network and identified each network's inflection point, for each

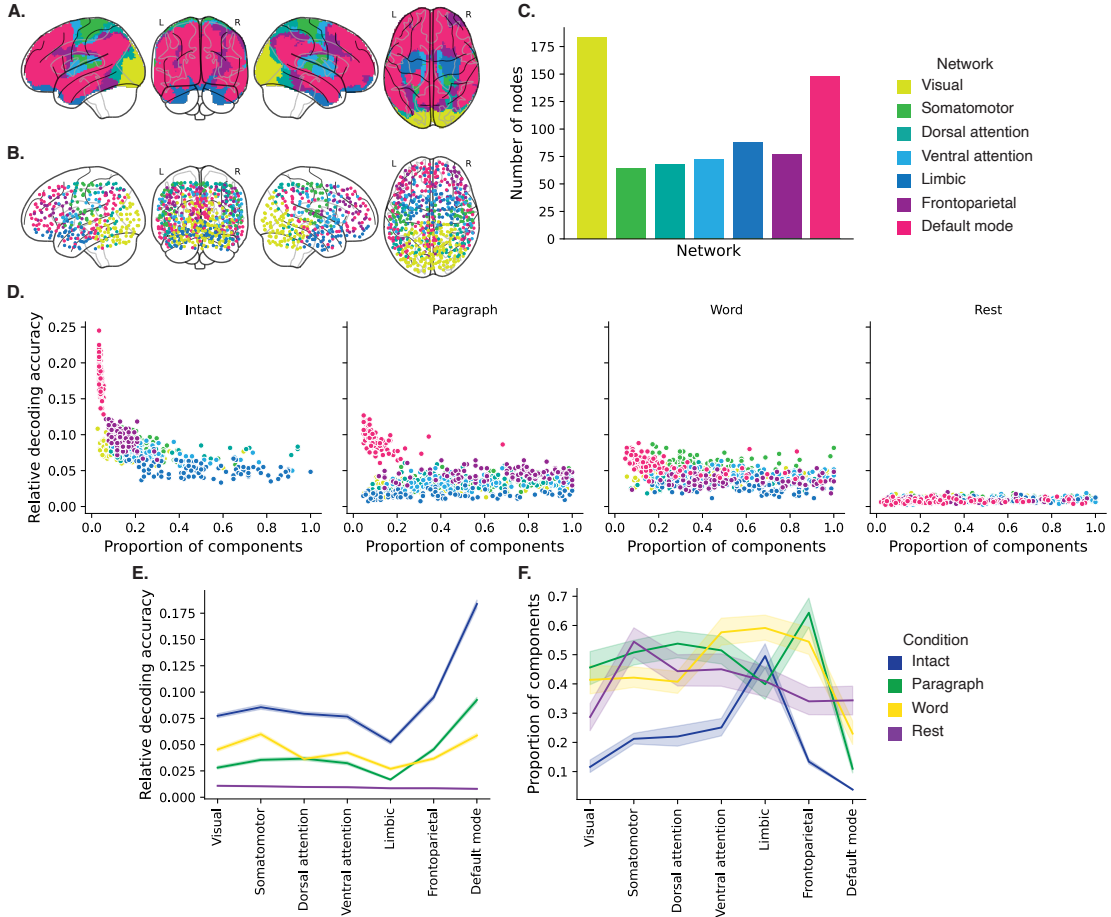


Figure 4: Network-specific decoding accuracy and compression. **A. Network parcellation map.** The glass brain displays the location of each of seven networks identified by Yeo et al. (2011). **B. Node labels.** We assigned network labels to each of 700 Hierarchical Topographic Factor Analysis-derived nodes (see *Hierarchical topographic factor analysis (HTFA)*). For each node, we evaluated its radial basis function (RBF) at the locations of every voxel in the parcellation map displayed in Panel A. We summed up these RBF weights separately for the voxels in each network. We defined each node's network label as its highest-weighted network across all voxels. **C. Per-network node counts.** The bar plot displays the total number of HTFA-derived nodes assigned to each network. **D. Informativeness versus compressibility by network and condition.** Each dot corresponds to a single cross validation run. The dots' coordinates denote the minimum proportion of components (relative to the number of nodes in the given network) required to achieve at least 5% corrected decoding accuracy (*x*-coordinate; for the rest condition these proportions are estimated using the peak decoding accuracies) and peak (corrected) decoding accuracy (*y*-coordinate). We repeated the analysis separately for each network (color) and experimental condition (column). **E. Informativeness by network.** For each network, sorted (roughly) from lower-order networks on the left to higher-order networks on the right, the curves display the peak (corrected) decoding accuracy for each experimental condition (color). **F. Compressibility by network.** For each network, the curves display the proportion of components (relative to the total possible number of components displayed in Panel C) required to achieve at least 5% decoding accuracy (or, for the rest condition, peak decoding accuracy, as described above). Error ribbons in Panels E and F denote bootstrap-estimated 95% confidence intervals.

experimental condition. Moving from low-order networks to higher-order networks, we found that decoding accuracy tended to increase, particularly in the higher-level experimental conditions (and decrease (slightly) in the lower-level experimental conditions (Fig. 4D, E; Spearman's rank correlation between decoding accuracy and network order: intact: $\rho = 0.362, p < 0.001$; paragraph: $\rho = 0.441, p < 0.001$; word: $\rho = -0.102, p = 0.007$; rest: $\rho = -0.354, p < 0.001$). This suggests that higher-order networks may carry more content-relevant or stimulus-driven "information." We found no clear trends in the proportions of components required to achieve 5% decoding accuracy across networks or conditions (Fig. 4F). We note that the limbic network we considered here often overlaps with low (imaging) signal regions, and therefore it may be difficult to draw strong conclusions about this network's informativeness or compressibility. We also considered the possibility that the correlations with network order might be influenced by the numbers of nodes in each network. We designed a permutation-based procedure to address this possibility, whereby we repeated the above analyses using shuffled network labels (see Network permutation tests). The correlations between decoding accuracy and network order were reliably more positive than the shuffled correlations for the intact ($t(1998) = 276.431, p < 0.001$) and paragraph ($t(1998) = 330.334, p < 0.001$) conditions, and reliably more negative for the word ($t(1998) = -16.386, p < 0.001$) and rest ($t(1998) = -318.631, p < 0.001$) conditions. These results suggest that the correlations between decoding accuracy and network order were not driven solely by the numbers of nodes in each network.

In addition to examining Whereas the above analyses examined different networks in isolation, we wondered about the general structure of the how does full-brain (i.e., potentially multi-network) activity patterns reflected by different principal components vary across different experimental conditions—? As shown in Figure 5, we used Neurosynth (Rubin et al., 2017) to identify, for each component, the associations with each of 80 themes (see Reverse inference). In general, the first principal components across all of the experimental conditions tended to weight weigh most heavily on themes related to cognitive control, memory, language processing, attention, and perception. Other components appeared to vary more across conditions.

To gain further insights into which brain functions might be most closely associated with the top-weighted components from each experimental condition, we manually grouped each Neurosynth-derived topic into a smaller set of core cognitive functions. Separately for each

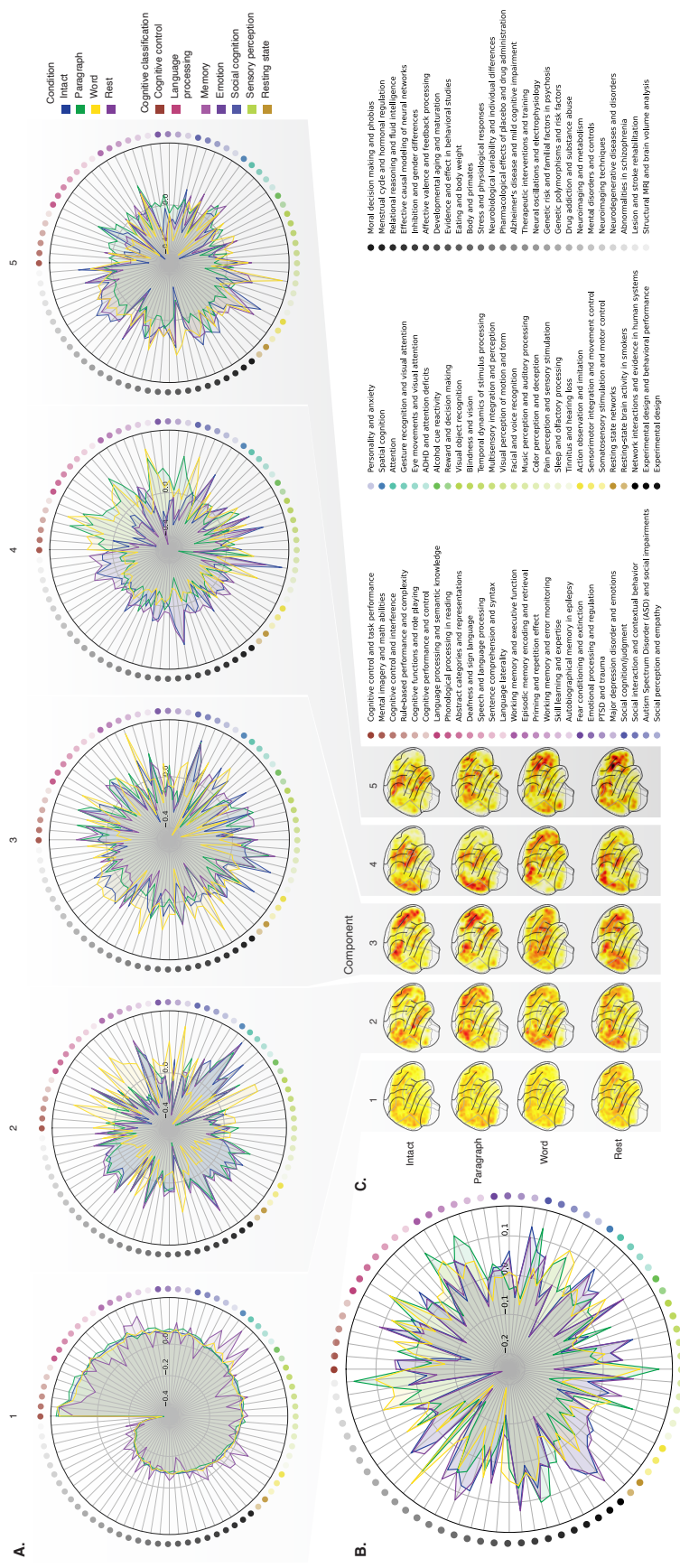


Figure 5: Neurosynth topic weightings by component. We used a reverse inference procedure (see *Reverse inference*) to estimate the correspondences between brain images and a set of 80 topics derived from the Neurosynth database of neuroimaging articles (Rubin et al., 2017). **A. Topic correlations by component.** For each of the top five highest-weighted principal components (columns) derived from each experimental condition (colors), the radar plots display the correlations between the component images and the per-topic images derived for each topic (topic identities are denoted by the blue dots; a legend for the topic labels is in the lower right of the figure). An annotated list of the top-weighted topics for each component and condition may be found in Figure S2 and the top-weighted terms for each topic may be found in Table S1. **B. Topic correlations averaged across components.** The radar plot is in the same format as the plots in Panel A, but here we display the per-condition average correlations across the top five components (for each condition) reflected in Panel A. **C. Component images.** Each plot displays a right sagittal view of a glass brain projection of the top five principal components (columns) for each experimental condition (rows). Additional projections for each component may be found in Figure S3.

component, we computed the average weightings across all topics that were tagged as being associated with each of these cognitive functions (Figs. 6A, S5A). To help visualize these associations, we used the patterns of associations for each component to construct graphs whose nodes were experimental conditions and cognitive functions (Figs. 6B, S5B). We also computed correlations between the sets of per-topic weightings from each of the top-weighted components from each experimental condition (Fig. 6C, D) and between the brain maps for each condition's components (Fig. S5C, D). Taken together, we found that each component appeared to ~~weight~~weigh on a fundamental set of cognitive functions that varied by experimental condition. For example, the top principal components from every condition ~~weighted~~weighed similarly (across conditions) on the full set of Neurosynth topics (Fig. 5A) and cognitive functions (Figs. 6A, B and S5 A, B), suggesting that these components might reflect a set of functions or activity patterns that are common across all conditions. The second components' weightings were similar across the intact, paragraph, and rest conditions (highest-weighted functions: cognitive control, memory, social cognition, and resting state), but different for the word condition (highest-weighted functions: sensory perception and cognitive control). The fourth components' weighting grouped the paragraph and word conditions (highest-weighted functions: memory, language processing, and cognitive control) and the intact and rest conditions (highest-weighted functions: emotion, social cognition). We also used ChatGPT (OpenAI, 2023) to sort the list of manually tagged cognitive functions from lowest-level to highest-level (Tab. S2, Fig. 6E; also see *Ranking cognitive processes*). We found that higher-level functions tended to be weighted ~~on~~ more heavily by top components from the intact and paragraph conditions than lower-level functions ~~—(intact vs.~~ word: $t(198) = 11.059, p < 0.001$; intact vs. rest: $t(198) = 3.699, p < 0.001$; paragraph vs. word: $t(198) = 13.504, p < 0.001$; paragraph vs. rest: $t(198) = 4.812, p < 0.001$; also see *Ranking cognitive processes*). The top components from the word condition showed the opposite tendency, whereby lower-level functions tended to be weighted ~~on~~ more heavily than higher-level functions ~~—The~~ (word vs. rest: $t(198) = -7.315, p < 0.001$). The weighting trends for the intact and paragraph conditions were not reliably different ($t(198) = -0.479, p = 0.633$). The components from the rest condition showed ~~almost no differences~~ only a small trending difference in the weights associated with high-level versus low-level functions ~~—(rest vs. 0: $t(99) = 1.836, p = 0.081$)~~. These findings suggest that when participants were engaged more strongly (in the more engaging intact and

287 paragraph conditions), their dominant neural patterns reflected higher-level cognitive functions.
288 In contrast, when participants were engaged less strongly (in the less engaging word and rest
289 conditions), their dominant neural patterns reflected lower-level cognitive functions. Although
290 they were highly statistically reliable, it is also important to note that these latter effects are also
291 relatively small (e.g., the slopes for *all* of the experimental conditions are numerically close to zero;
292 Fig. 6E). We suggest that this phenomenon may merit further investigation in future work.

293 Discussion

294 We examined fMRI data collected as participants listened to an auditory recording of a story, scram-
295 bled recordings of the story, or underwent a resting state scan. We found that cognitively richer
296 stimuli evoked more reliable (i.e., consistent across people) and information rich brain activity pat-
297 terns. The brain patterns evoked by cognitively richer stimuli were also more compressible, in that
298 each individual component provided more “signal” to temporal decoders relative to components
299 of data from less cognitively rich conditions (Fig. 2). Over time (e.g., as the experiment progressed),
300 these phenomena were strengthened. Specifically, across story segments, data from more cogni-
301 tively rich conditions became more informative and compressible, and data from less cognitively
302 rich conditions became *less* informative and compressible (Fig. 3). We also repeated these analyses
303 separately for different brain networks. We found that networks traditionally associated with
304 higher-level cognitive functions tended to provide more informative brain patterns than networks
305 traditionally associated with lower level cognitive functions (Fig. 4). Finally, we examined the most
306 dominant components of the brain activity patterns from each experimental condition. We used a
307 reverse inference approach (Rubin et al., 2017) to identify the terms in the neuroimaging literature
308 most commonly associated with the corresponding maps. As summarized in Figure 6E, we found
309 that the intact and paragraph conditions tended to weight ~~on~~-higher-level cognitive processes
310 more than lower-level cognitive processes, whereas the word condition weighted ~~on~~-lower-level
311 processes more than higher-level processes and the rest condition showed no reliable difference in
312 high-level versus low-level ~~weighting~~weightings. Taken together, our findings indicate that the
313 informativeness and compressibility of our brain activity patterns are task-dependent, and these
314 properties change systematically with factors like cognitive richness and depth of processing.

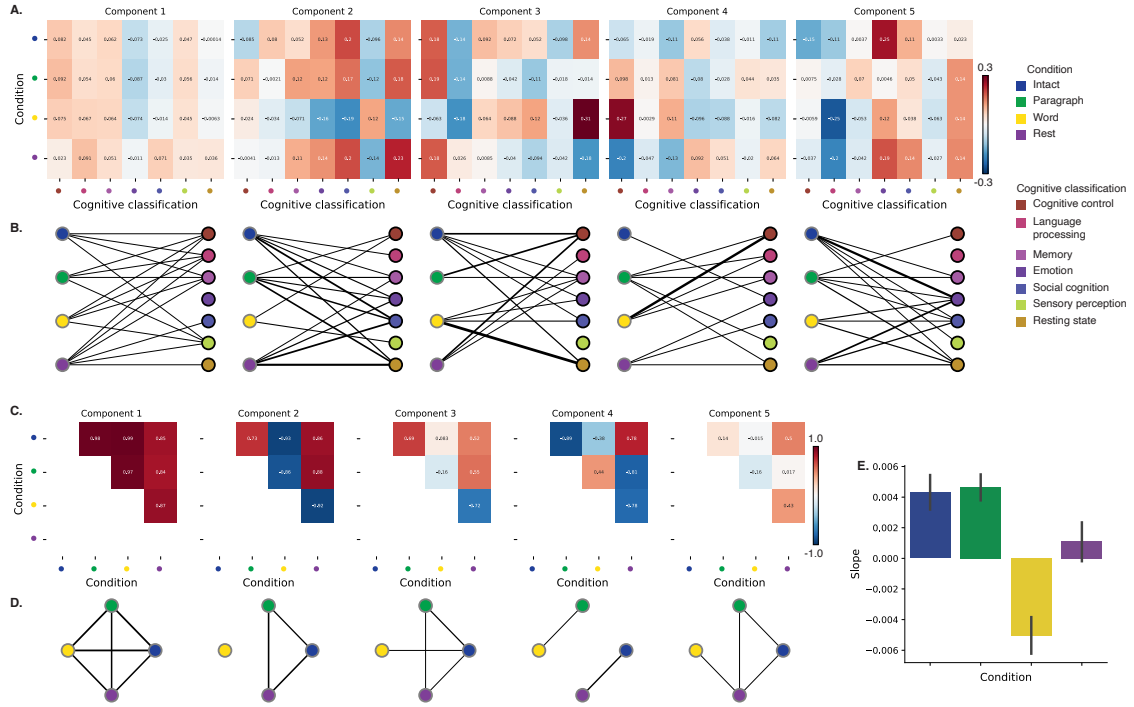


Figure 6: Summary of functions associated with top-weighted components by condition. A. Top-weighted topics by condition. Here we display per-condition (rows, indicated by colored dots) topic correlations, averaged across topics that pertain to each of several broad cognitive functions (columns within each sub-panel, indicated by colored dots). Each sub-panel reflects correlations for the components indicated in the panel titles. **A legend for the condition and several core cognitive function classifications is displayed in the lower right of the figure.** Table S1 provides a list of each topic’s top-weighted terms, along with each topic’s manually labeled cognitive classification. A full list of the topics most highly associated with each component may be found in Figure S2. **B. Associations between per-condition components and cognitive functions.** The network plots denote positive average correlations between the component images for each condition (gray-outlined dots on the left sides of each network; colors denote conditions) and topic-specific brain maps associated with each indicated cognitive function (black-outlined dots on the right sides of each network; colors denote cognitive functions). The line thicknesses are proportional to the correlation values (correlation coefficients are noted in the heat maps in Panel A). **C. Correlations between each principal component, by condition.** The heat maps display the correlations between the brain maps (Fig. S3) for each principal component (sub-panel), across each pair of conditions (rows and columns of each sub-panel’s matrix, indicated by colored dots). **D. Associations between per-condition components, by component.** Each sub-panel’s network plot summarizes the pattern of correlations between the n^{th} top-weighted principal components (sub-panel) for each experimental condition (gray-outlined dots). The line thicknesses are proportional to the correlation values (correlation coefficients are noted in the heat maps in Panel C). **E. Change in weights by condition.** The bar heights reflect the slopes of regression lines, fit separately to the top five components from each condition, between the ChatGPT-derived “rank” of each cognitive classification and the correlations between the component and topic maps associated with cognitive processes at the given rank (see *Ranking cognitive processes*) **Error bars denote bootstrap-estimated 95% confidence intervals.** Also see Fig. S5 for additional information.

315 Our explorations of informativeness and compressibility are related to a much broader literature
316 on the correlational and causal structure of brain activity patterns and networks (Adachi et
317 al., 2012; Bassett & Sporns, 2017; Brovelli et al., 2004; Bullmore & Sporns, 2009; Dhamala et al.,
318 2008; Korzeniewska et al., 2008; Lynn & Bassett, 2021; Owen et al., 2021; Preti et al., 2017; Rogers
319 et al., 2007; Rubinov & Sporns, 2010; Sizemore et al., 2018; Smith, Beckmann, et al., 2013; Smith,
320 Vidaurre, et al., 2013; Sporns & Betzel, 2016; Sporns & Honey, 2006; Sporns & Zwi, 2004; Srinivasan
321 et al., 2007; Tomasi & Volkow, 2011; Yeo et al., 2011). Correlations or causal associations between
322 different brain regions simultaneously imply that full-brain activity patterns will be compressible
323 and also that those activity patterns will contain redundancies. For example, the extent to which
324 activity patterns at one brain area can be inferred or predicted from activity patterns at other
325 areas (e.g., Owen et al., 2020; Scangos et al., 2021), reflects overlap in the information available
326 in or represented by those brain areas. If brain patterns in one area are recoverable using brain
327 patterns in another area, then a “signal” used to convey the activity patterns could be compressed
328 by removing the recoverable activity. Predictable (and therefore redundant) brain activity patterns
329 are also more robust to signal corruption. For example, even if the activity patterns at one region
330 are unreadable or unreliable at a given moment, that unreliability could be compensated for by
331 other regions’ activity patterns that were predictive of the unreliable region. Whereas compressible
332 brain patterns are robust to spatial signal corruption, high versus low informativeness reflects a
333 similar (though dissociable; e.g., Fig. 1) tradeoff between expressiveness and robustness of temporal
334 patterns. Highly informative brain patterns (by our measure; i.e., patterns that yield greater
335 temporal decoding accuracy) are expressive about ongoing experiences or cognitive states, since
336 each moment’s pattern is reliably distinguishable from other moments’ patterns. However, when
337 each moment’s pattern is unique, brain activity becomes less robust to temporal signal corruption.
338 Our finding that brain activity patterns becomes more informative (i.e., less robust to temporal
339 signal corruption) and compressible (i.e., more robust to spatial signal corruption) when cognitive
340 engagement is higher suggests that our brain may optimize its activity patterns to prioritize either
341 temporal or spatial robustness, according to task demands.

342 Our findings that informativeness and compressibility change with task demands may follow
343 from task-dependent changes in full-brain correlation patterns. A number of prior studies have
344 found that so-called “functional connectivity” (i.e., correlational) patterns vary reliably across

345 tasks, events, and situations (Cole et al., 2014; Owen et al., 2021; Simony et al., 2016; Smith et
346 al., 2009). By examining how these task-dependent changes in correlations affect informativeness
347 and compressibility, our work suggests a potential reason why the statistical structure of brain
348 activity patterns might vary with cognitive task or with cognitive demands. For lower-level tasks,
349 or for tasks that require relatively little “deep” cognitive processing, our brains may optimize
350 activity patterns for robustness and redundancy over expressiveness, for example to maximize
351 reliability. For higher-level tasks, or for tasks that require deeper cognitive processing, our brains
352 may sacrifice some redundancy in favor of greater expressiveness.

353 **In the information** One potential limitation of our work concerns how our measure of informativeness
354 might generalize across different tasks, cognitive representations, and processes. Our use of
355 across-participant temporal decoding accuracy as a proxy for informativeness is motivated in part
356 by prior work that introduced across-participant similarity (in time-varying response to a stimulus)
357 as a means of identifying stimulus-driven brain activity patterns (Simony et al., 2016). Intuitively,
358 only activity patterns that are driven by the stimulus would be expected to synchronize (i.e., be
359 time-locked to the stimulus) across participants. This approach implicitly removes idiosyncratic
360 responses (e.g., neural patterns that are *not* similar across people). However, there are also
361 some published examples, including in our own prior work, that indicate that some types of
362 stimulus-evoked activity will be missed by across-participant comparisons. For example we have
363 reported how brain regions like the ventromedial prefrontal cortex (vmPFC) show stimulus-driven
364 responses that are, for the most part, *not* similar across people. In that paper (and drawing on other
365 work), we suggest that the vmPFC seems to represent or support highly idiosyncratic internal
366 states, like affective responses. Although we would consider the vmPFC to be a “high-level”
367 region (e.g., we consider affect to be a relatively high-level aspect of cognition), the measure of
368 informativeness that we used in our current study would identify regions like the vmPFC as having
369 *low* informativeness. This is because across-participant decoding accuracy (our proxy measure for
370 informativeness) will only be high for representations or responses that are common across people.

371

372 Relatedly, even in the experimental conditions we describe as “less cognitively engaging,” we
373 think it likely that high-level thought or cognitive processing is still present. Rather, we suggest
374 that these high-level representations will tend to be more idiosyncratic when the stimulus is less

375 engaging, and therefore less constraining on people's thoughts. Nonetheless, even during highly
376 engaging tasks, people may engage in idiosyncratic stimulus-driven processes. For example,
377 people might retrieve personal information as they listened to the story. Those retrievals could
378 happen at different times for different people according to each individual's prior experiences.
379 Even when those sorts of retrievals happen to be temporally synchronized across people, the
380 specific memories or information being retrieved might still be idiosyncratic. Our measure
381 of informativeness is insensitive to these processes. Further, even in response to an identical
382 stimulus, task instructions or participants' internal goals could change the relationship between
383 compressibility and informativeness. Some work has shown that the "dimensionality" of neural
384 representations can change systematically with task complexity, even in response to an identical
385 stimulus (Mack et al., 2020). Taken together, we expect that the way we have defined informativeness
386 in this paper, and the specific dataset we examined, are likely to have influenced our findings.
387 While we see our approach as a reasonable first step, we also suggest that future work should
388 explore alternative measures of informativeness and compressibility, and should examine how
389 these measures vary across different tasks and datasets.

390 In the information theory sense (Shannon, 1948), when a signal is transmitted using a fixed
391 alphabet of "symbols," the information rate decreases as the signal is compressed (e.g., fewer sym-
392 bols transmitted per unit time, using an alphabet with fewer symbols, etc.). Our finding that each
393 individual brain component (symbol) becomes more informative as cognitive richness increases
394 suggests that the "alphabet" of brain activity patterns is also task-dependent. Other work suggests
395 that the representations that are *reflected* by brain activity patterns may also change with task de-
396 mands. For example, our brains may represent the same perceptual stimulus differently depending
397 on which aspects of the stimulus or which combinations of features are task-relevant (Mack et al.,
398 2020).

399 **Different brain networks also** We found that different brain networks varied in how informative
400 and compressible their activity patterns were across experimental conditions (e.g., Fig. 4). This
401 might follow from evolutionary optimizations that reflect the relevant constraints or demands
402 placed on those networks. One possibility is that cortex is organized in a hierarchy of networks
403 "concerned with" or selective to different levels of processing or function. To the extent that
404 different levels of processing (e.g., low-level sensory processing versus "deeper" higher-level pro-

cessing) reflect different stimulus timescales (e.g., Manning, 2023), the network differences we observed might also relate to the timescales at which each network is maximally sensitive (Baldassano et al., 2017; Hasson et al., 2008; Lerner et al., 2011; Regev et al., 2018).

Our reverse inference analyses (Figs. 5, 6) also provide some insights into how neural activity patterns change with cognitive engagement or task demands. Prior work has shown that the components and network “parcels” identified through covarying activity patterns can be highly similar even across different tasks (including “rest,” e.g., Laird et al., 2011; Smith et al., 2009). We replicated this basic finding in that the first principal components from all four experimental conditions were strikingly similar (e.g., see the leftmost columns of Figs. 5A and 6C, D). We also found some small, though statistically reliable, systematic changes in the weights associated with different cognitive functions across conditions (Fig. 6E). This result provided an additional way of characterizing network-level differences across conditions (Fig. 4E). Taken together, these findings suggest that although similar networks may be involved in different tasks, the ways in which those networks are engaged may vary systematically with task demands.

Concluding remarks

Cognitive neuroscientists are still grappling with basic questions about the fundamental “rules” describing how our brains respond, and about how brain activity patterns and the associated underlying cognitive representations and computations are linked. We identified two aspects of brain activity patterns, informativeness and compressibility, that appear to change systematically with task demands and across brain networks. Our work helps to clarify how the “neural code” might be structured, and how the code might vary across tasks and brain areas. We speculate that these changes may reflect ongoing tradeoffs between how robust to signal corruption versus how expressive about ongoing cognitive states our brains’ activity patterns are. Our work also provides a new framework for evaluating these tradeoffs in other datasets, or in future studies.

Methods

We measured properties of recorded neuroimaging data under different task conditions that varied systematically in cognitive engagement and depth of processing. We were especially interested in

432 how informative and compressible the activity patterns were under these different conditions (Fig. 1).
433 Unless otherwise noted, all statistical tests are two-sided, all error bars and error ribbons
434 denote bootstrap-estimated 95% confidence intervals across participants, and all reported *p*-values
435 are corrected for multiple comparisons using the Benjamini-Hochberg procedure (Benjamini &
436 Hochberg, 1995).

437 **Functional neuroimaging data collected during story listening**

438 We examined an fMRI dataset collected by Simony et al. (2016) that the authors have made publicly
439 available at arks.princeton.edu/ark:/88435/dsp015d86p269k. The dataset comprises neuroimaging
440 data collected as participants listened to an audio recording of a story (intact condition; 36 par-
441 ticipants), listened to temporally scrambled recordings of the same story (17 participants in the
442 paragraph-scrambled condition listened to the paragraphs in a randomized order and 36 in the
443 word-scrambled condition listened to the words in a randomized order), or lay resting with their
444 eyes open in the scanner (rest condition; 36 participants). Full neuroimaging details may be found
445 in the original paper for which the data were collected (Simony et al., 2016). Procedures were
446 approved by the Princeton University Committee on Activities Involving Human Subjects, and by
447 the Western Institutional Review Board (Puyallup, WA). All subjects were native English speakers
448 with normal hearing and provided written informed consent. We have excerpted the relevant
449 portions of the dataset documentation here to provide information about the scanning parameters
450 and preprocessing steps used to generate the data we analyzed (the original descriptions may be
451 found at the above link):

452 Subjects were scanned in a 3T full-body MRI scanner (Skyra; Siemens) with a sixteen-channel
453 head coil. For functional scans, images were acquired using a T2* weighted echo planer
454 imaging (EPI) pulse sequence [repetition time (TR), 1500 ms; echo time (TE), 28 ms;
455 flip angle, 64°], each volume comprising 27 slices of 4 mm thickness with 0 mm gap;
456 slice acquisition order was interleaved. In-plane resolution was 3 × 3 mm² [field of
457 view (FOV), 192 × 192 mm²]. Anatomical images were acquired using a T1-weighted
458 magnetization-prepared rapid-acquisition gradient echo (MPRAGE) pulse sequence
459 (TR, 2300 ms; TE, 3.08 ms; flip angle 9°; 0.89 mm³ resolution; FOV, 256 mm²). To

460 minimize head movement, subjects' heads were stabilized with foam padding. Stimuli
461 were presented using the Psychophysics toolbox (Brainard, 1997; Pelli, 1997). Subjects
462 were provided with an MRI compatible in-ear mono earbuds (Sensimetrics Model S14),
463 which provided the same audio input to each ear. MRI-safe passive noise-canceling
464 headphones were placed over the earbuds, for noise removal and safety.

465 Functional data were preprocessed and analyzed using FSL (www.fmrib.ox.ac.uk/fsl),
466 including correction for head motion and slice-acquisition time, spatial smoothing
467 (6 mm FWHM Gaussian kernel), and high-pass temporal filtering (140 s period).
468 Preprocessed data were aligned to coplanar and high-resolution anatomicals and the
469 standard MNI152 brain, and interpolated to 3-mm isotropic voxels.

470 The intact and word conditions each comprised 300 TRs (7.5 minutes) per participant. The
471 paragraph condition comprised 272 TRs (6.8 minutes) per participant. The rest condition comprised
472 400 TRs (10 minutes) per participant.

473 Hierarchical topographic factor analysis (HTFA)

474 Following our prior related work, we used HTFA (Manning et al., 2018) to derive a compact
475 representation of the neuroimaging data. In brief, this approach approximates the timeseries
476 of voxel activations (44,415 voxels) using a much smaller number of radial basis function (RBF)
477 nodes (in this case, 700 nodes, as determined by an optimization procedure; Manning et al., 2018).
478 This provides a convenient representation for examining full-brain activity patterns and network
479 dynamics. All of the analyses we carried out on the neuroimaging dataset were performed in
480 this lower-dimensional space. In other words, each participant's data matrix was a number-of-
481 timepoints (T) by 700 matrix of HTFA-derived factor weights (where the row and column labels
482 were matched across participants). Code for carrying out HTFA on fMRI data may be found as
483 part of the BrainIAK toolbox (Capota et al., 2017; Kumar et al., 2021), which may be downloaded
484 at brainiak.org.

485 We also considered alternative approaches to obtaining compact representations of the neuroimaging
486 data, including network parcellations (e.g., Gordon et al., 2016; Schaefer et al., 2018). Whereas
487 network parcellations are typically derived from large resting state datasets, HTFA may be applied

488 to much smaller datasets. In our prior work, we showed that HTFA applied to the same dataset
489 used here can explain full-brain activity to within a maximum of 0.25 standard deviations of each
490 voxel's observed activity in the original dataset, taken across all voxels, images, and participants,
491 using the 700-node representation we also employed here (Manning et al., 2018). Some of the
492 explanatory power of HTFA comes from the fact that each node's influence falls off smoothly with
493 distance to its center. Intuitively, the result is a representation that looks like a lightly spatially
494 smoothed version of the original data, but where the degree of smoothing varies across the brain
495 according to how spatially autocorrelated the local activity patterns are.

496 **Network permutation tests**

497 In our analyses of how informativeness varied across brain networks (Fig. 4), we considered the
498 possibility that the correlations with network order might be influenced by the numbers of nodes
499 in each network. We designed a permutation-based procedure to address this possibility, whereby
500 we repeated the above analyses using shuffled network labels. Specifically, for each of $n_1 = 10$
501 iterations, we randomly shuffled (without replacement) the network labels of the HTFA nodes, and
502 then we re-ran our entire decoding analysis pipeline, including applying PCA with $3 \dots m$ features
503 for each condition (where m is the number of nodes in the given network), and then running 100
504 cross-validation runs of the decoding procedure for each condition and number of components.
505 This resulted in 10 sets of shuffled data, where each network had the same numbers of nodes, but
506 where the decoding results no longer maintained the fidelity of each individual network.

507 We sampled the original and shuffled datasets (with replacement) to create $n_2 = 1000$ bootstrap
508 samples. For each bootstrap sample, we computed the correlations between the decoding accuracies
509 and network order for each condition and number of components. This yielded a distribution of
510 n_2 correlation values for each condition, for both the original and shuffled datasets. We then
511 compared the distributions of Spearman's ρ values for the original and shuffled datasets using
512 two-sided independent samples Welch's t -tests.

513 **Principal components analysis (PCA)**

514 We applied group PCA (Smith et al., 2014) separately to the HTFA-derived representations of the
515 data (i.e., factor loadings) from each experimental condition. Specifically, for each condition, we
516 considered the set of all participants' T by 700 factor weight matrices. We used group PCA to project
517 these 700-dimensional matrices into a series of shared k -dimensional spaces, for $k \in \{3, 4, 5, \dots, 700\}$.
518 This yielded a set of number-of-participants matrices, each with T rows and k columns.

519 **Temporal decoding**

520 We sought to identify neural patterns that reflected participants' ongoing cognitive processing of
521 incoming stimulus information. As reviewed by Simony et al. (2016), one way of homing in on
522 these stimulus-driven neural patterns is to compare activity patterns across individuals. In partic-
523 ular, neural patterns will be similar across individuals to the extent that the neural patterns under
524 consideration are stimulus-driven, and to the extent that the corresponding cognitive representa-
525 tions are reflected in similar spatial patterns across people (Simony & Chang, 2020). Following this
526 logic, we used an across-participant temporal decoding test developed by Manning et al. (2018) to
527 assess the degree to which different neural patterns reflected ongoing stimulus-driven cognitive
528 processing across people. The approach entails using a subset of the data to train a classifier to
529 decode stimulus timepoints (i.e., moments in the story participants listened to) from neural pat-
530 terns. We use decoding (forward inference) accuracy on held-out data, from held-out participants,
531 as a proxy for the extent to which the inputted neural patterns reflected stimulus-driven cognitive
532 processing in a similar way across individuals.

533 **Forward inference and decoding accuracy**

534 We used an across-participant correlation-based classifier to decode which stimulus timepoint
535 matched each timepoint's neural pattern. For a given value of k (i.e., number of principal compo-
536 nents), we first used group PCA to project the data from each condition into a shared k -dimensional
537 space. Next, we divided the participants into two groups: a template group, $\mathcal{G}_{\text{template}}$ (i.e., training
538 data), and a to-be-decoded group, $\mathcal{G}_{\text{decode}}$ (i.e., test data). We averaged the projected data within
539 each group to obtain a single T by k matrix for each group. Next, we correlated the rows of the two

540 averaged matrices to form a T by T decoding matrix, Λ . In this way, the rows of Λ reflected time-
541 points from the template group, while the columns reflected timepoints from the to-be-decoded
542 group. We used Λ to assign temporal labels to each timepoint (row) from the test group's ma-
543 trix, using the row of the training group's matrix with which it was most highly correlated. We
544 repeated this decoding procedure, but using $\mathcal{G}_{\text{decode}}$ as the template group and $\mathcal{G}_{\text{template}}$ as the
545 to-be-decoded group. Given the true timepoint labels (for each group), we defined the decoding
546 accuracy as the average proportion of correctly decoded timepoints, across both groups (where
547 chance performance is $\frac{1}{T}$). In Figures 2 and 3 we report the decoding accuracy for each condition
548 and value of k , averaged across $n = 100$ cross validation folds.

549 **Reverse inference**

550 To help interpret the brain activity patterns we found within the contexts of other studies, we
551 created summary maps of each principal component, for each experimental condition. Each
552 principal component comprises 700 “weights” on each of the HTFA-derived RBF nodes (see
553 *Hierarchical Topographic Factor Analysis*). For each node, we evaluated its RBF at the locations of
554 every voxel in the standard 2 mm MNI152 template brain and multiplied the RBF by the node’s
555 weight. The sum of these weighted RBF activation maps provides a full-brain image, in MNI152
556 space, of the given principal component (Fig. S3).

557 Next, we considered 80 topics estimated using Latent Dirichlet Allocation (Blei et al., 2003)
558 applied to 9,204 functional neuroimaging articles in the Neurosynth database (Rubin et al., 2017).
559 The topics, as well as associated brain maps identified using Neurosynth, were identified and
560 reported in several prior studies (Chen et al., 2020; Fox et al., 2014; Sul et al., 2017). The topic
561 labels for each topic were generated automatically with the following ChatGPT (OpenAI, 2023)
562 prompt: “Please help me come up with intuitive labels for topics I found by fitting a topic model
563 to thousands of neuroscience and psychology articles. I’ll paste in the top 10 highest-weighted
564 words for each topic, and I’d like you to respond with a suggested label. For each topic, please
565 respond with just the topic label and no other formatting or text. Here are the next topic’s top
566 words:” followed by a comma-separated list of the given topic’s top-weighted words reflected
567 in the Table S1. For some topics, ChatGPT responded with a longer-form response rather than a

568 concise topic label. In these instances, on a case-by-case basis, we used a second follow-up prompt
569 to achieve the given topic's label: "Could you please come up with a more concise label for that
570 topic?". We then manually identified a set of 11 cognitive labels that were intended to encapsulate
571 a representative range of widely studied low-level and high-level cognitive functions. In choosing
572 the set of cognitive labels, we jointly considered each topic's ChatGPT-derived topic label, along
573 with the top-weighted words for the topic. We attempted to generate a concise set of labels that
574 still spanned the full set of cognitive functions reflected across the 80 topics. Topics that appeared
575 unrelated to specific cognitive functions (e.g., topics related to specific methods or clinical themes)
576 are designated with dashes in Table S1.

577 Finally, following an approach used in several prior studies (Chen et al., 2020; Fox et al., 2014;
578 Sul et al., 2017) we treated the correlation between a given component's brain map and each topic's
579 brain map as an approximate measure of how much the component was reflective of the given
580 topic. This resulted in a set of 80 "weights" (correlation coefficients) for each component's brain
581 map, with one weight per Neurosynth-derived topic.

582 Ranking cognitive processes

583 We manually identified 11 cognitive labels spanning the set of 80 Neurosynth-derived topics:
584 cognitive control, language processing, memory, emotion, social cognition, spatial cognition, at-
585 tention, reward, sensory perception, motor control, and resting state. We then used ChatGPT
586 to automatically "rank" the processes from high-level to low-level using the following prompt:
587 "Please rank these cognitive processes from highest-level to lowest-level, where higher values
588 indicate higher-order or higher-level processes. Return the result as a csv file with a header row
589 and two columns: 'Cognitive label' and 'Rank'. Here are the processes: cognitive control, lan-
590 guage processing, memory, emotion, social cognition, spatial cognition, attention, reward, sensory
591 perception, motor control, resting state". Table S2 displays the output. ~~We used these labels in the~~

592 We recognize that ChatGPT is not omniscient, nor should it be treated as an expert cognitive
593 neuroscientist. We therefore reviewed ChatGPT's responses carefully by hand to verify that they
594 seemed reasonable to us. Whereas prior work has often constructed such rankings by hand, we see
595 our use of ChatGPT in this case as a small additional "sanity check" on our rankings that helped

596 us to be slightly more objective than if we had simply created the rankings ourselves manually.
597 In the analysis presented in Figure 6E~~to help~~, we summarize difference in topic weightings
598 across experimental conditions. In particular, we sought to characterize how the dominant neural
599 patterns evoked by each experimental condition weighted on different cognitive functions. For
600 each of the top five principal components from each experimental condition (Fig. 5), we computed
601 the average weights for each of the 11 manually identified (and ChatGPT-ranked) cognitive labels
602 described above (Tab. S2). We then fit a line separately for each experiment condition (x -values:
603 cognitive rank; y -values: weights). In carrying out this analysis, we used a bootstrap procedure
604 to estimate the variability in the slopes of the regression lines, whereby we repeated this process
605 for each of $n = 100$ iterations, each time resampling (with replacement) the set of observed ranks
606 and weights. This procedure yielded distributions of 100 estimated slopes for each experimental
607 condition. We used these distributions to compare the slopes across experimental conditions and
608 to estimate 95% confidence intervals.

609 **Synthetic data**

610 To help illustrate the relationship between informativeness and compressibility (Fig. 1), we generated
611 four synthetic datasets, varying in informativeness and compressibility. Each dataset comprised
612 simulated observations of $K = 25$ features across $N = 100$ timepoints, from each of $S = 10$ participants.
613 To create each dataset, we first constructed a “template” matrix of N timepoints by K features. We
614 then generated participant-specific data by adding independent noise to each entry in template
615 matrix, drawn from the unit normal distribution (i.e., with a mean of 0 and a variance of 1). We
616 repeated this process for each participant, yielding S participant-specific matrices for each dataset.
617

618 Since we estimate informativeness using the temporal decoding accuracy across participants,
619 highly informative data will tend to have observations that are highly timepoint specific. Relatively
620 uninformative data, in contrast, will tend to have more similar observations across timepoints.
621 To generate data with “high informativeness,” we constructed template matrices whose rows
622 (observations) were drawn independently from zero-mean multivariate normal distributions.
623 The covariances of these distributions were determined according to the desired compressibility

624 of the data, as described below. We used a multi-step process to generate data with “low
625 informativeness.” First we generated new template matrices using the same procedure as for
626 the “high informativeness” datasets. We then multiplied each matrix by a constant ($\rho = 0.1$) and
627 computed the cumulative sum of each matrix’s rows. This yielded matrices whose rows were
628 highly similar across observations.

629 Compressibility reflects the extent to which decoding accuracy is affected by reducing the
630 number of components used to represent the data. Highly compressible data will tend to
631 exhibit more similarities across features, whereas less compressible data will tend to show greater
632 independence across features. To generate data with “high compressibility,” we set the covariance
633 matrix of the multivariate normal distribution to a toeplitz matrix whose first row was given by
634 $[K, K-1, \dots, 1]$. To generate data with “low compressibility,” we set the covariance matrix to the
635 identity matrix.

636 Template matrices for datasets with high informativeness and high compressibility, high
637 informativeness and low compressibility, low informativeness and high compressibility, and low
638 informativeness and low compressibility are displayed in Figure 1C. The corresponding decoding
639 curves are displayed in Figure 1D.

640 Data and code availability

641 All of the code used to produce the figures and results in this manuscript, along with links to the
642 corresponding data, may be found at github.com/ContextLab/pca_paper.

643 Acknowledgements

644 We acknowledge discussions with Rick Betzel, Luke Chang, Emily Finn, and Jim Haxby. Our
645 work was supported in part by NSF CAREER Award Number 2145172 to J.R.M. The content is
646 solely the responsibility of the authors and does not necessarily represent the official views of our
647 supporting organizations. The funders had no role in study design, data collection and analysis,
648 decision to publish, or preparation of the manuscript.

649 **Author contributions**

650 Conceptualization: J.R.M. and L.L.W.O. Methodology: J.R.M. and L.L.W.O. Implementation:
651 J.R.M. and L.L.W.O. Analysis: J.R.M. and L.L.W.O. Writing, Reviewing, and Editing: J.R.M. and
652 L.L.W.O. Funding acquisition: J.R.M. Supervision: J.R.M.

653 **References**

- 654 Adachi, Y., Osada, T., Sporns, O., Watanabe, T., Matsui, T., Miyamoto, K., & Miyashita, Y.
655 (2012). Functional connectivity between anatomically unconnected areas is shaped by collective
656 network-level effects in the macaque cortex. *Cerebral Cortex*, 22(7), 1586–1592.
- 657 Alvarez, S. A. (2002). *An exact analytical relation among recall, precision, and classification accuracy in
658 information retrieval* (Technical Report No. BCCS-02-01). Boston College.
- 659 Baldassano, C., Chen, J., Zadbood, A., Pillow, J. W., Hasson, U., & Norman, K. A. (2017). Discov-
660 ering event structure in continuous narrative perception and memory. *Neuron*, 95(3), 709–721.
- 661 Bassett, D. S., & Sporns, O. (2017). Network neuroscience. *Nature Neuroscience*, 20(3), 353–364.
- 662 Benjamini, Y., & Hochberg, Y. (1995). Controlling the False Discovery Rate: a practical and
663 powerful approach to multiple testing. *Journal of Royal Statistical Society, Series B*, 57, 289–300.
- 664 Blei, D. M., Ng, A. Y., & Jordan, M. I. (2003). Latent dirichlet allocation. *Journal of Machine Learning
665 Research*, 3, 993–1022.
- 666 Brainard, D. H. (1997). The psychophysics toolbox. *Spatial Vision*, 10, 443–446.
- 667 Brovelli, A., Ding, M., Ledberg, A., Chen, Y., Nakamura, R., & Bressler, S. (2004). Beta oscillations in
668 a large-scale sensorimotor cortical network: directional influences revealed by Granger causality.
669 *Proceedings of the National Academy of Sciences, USA*, 101(26), 9849–9854.
- 670 Bullmore, E., & Sporns, O. (2009). Complex brain networks: graph theoretical analysis of structural
671 and functional systems. *Nature Reviews Neuroscience*, 10(3), 186–198.

- 672 Capota, M., Turek, J., Chen, P.-H., Zhu, X., Manning, J. R., Sundaram, N., ... Shin, Y. S. (2017).
673 *Brain imaging analysis kit.*
- 674 Chen, P.-H. A., Jolly, E., Cheong, J. H., & Chang, L. J. (2020). Intersubject representational
675 similarity analysis reveals individual variations in affective experience when watching erotic
676 movies. *NeuroImage*, 216(116851), doi.org/10.1016/j.neuroimage.2020.116851.
- 677 Cole, M. W., Bassett, D. S., Power, J. D., Braver, T. S., & Petersen, S. E. (2014). Intrinsic and
678 task-evoked network architectures of the human brain. *Neuron*, 83(1), 238–251.
- 679 Dhamala, M., Rangarajan, G., & Ding, M. (2008). Analyzing information flow in brain networks
680 with nonparametric Granger causality. *NeuroImage*, 41(2), 354–362.
- 681 Finn, E. S., Scheinost, D., Finn, D. M., Shen, X., Papademetris, X., & Constable, R. T. (2017).
682 Can brain state be manipulated to emphasize individual differences in functional connectivity.
683 *NeuroImage*, 160, 140–151.
- 684 Finn, E. S., Shen, X., Scheinost, D., Rosenberg, M. D., Huang, J., Chun, M. M., ... Constable, R. T.
685 (2015). Functional connectome fingerprinting: identifying individuals using patterns of brain
686 connectivity. *Nature Neuroscience*, 18, 1664–1671.
- 687 Fox, A. S., Chang, L. J., Gorgolewski, K. J., & Yarkoni, T. (2014). Bridging psychology and
688 genetics using large-scale spatial analysis of neuroimaging and neurogenetic data. *bioRxiv*,
689 doi.org/10.1101/012310.
- 690 Glerean, E., Salmi, J., Lahnakoski, J. M., Jääskeläinen, I. P., & Sams, M. (2012). Functional magnetic
691 resonance imaging phase synchronization as a measure of dynamic functional connectivity.
692 *Brain Connectivity*, 2(2), 91–101.
- 693 Gordon, E. M., Laumann, T. O., Adeyemo, B., Huckins, J. F., Kelley, W. M., & Petersen, S. E. (2016).
694 Generation and evaluation of a cortical area parcellation from resting-state correlations. *Cerebral
695 Cortex*, 26, 288–303.
- 696 Gratton, C., Laumann, T. O., Nielsen, A. N., Greene, D. J., Gordon, E. M., Gilmore, A. W., ...
697 Petersen, S. E. (2018). Functional brain networks are dominated by stable group and individual
698 factors, not cognitive or daily variation. *Neuron*, 98(2), 439–452.

- 699 Hasson, U., Yang, E., Vallines, I., Heeger, D. J., & Rubin, N. (2008). A hierarchy of temporal
700 receptive windows in human cortex. *The Journal of Neuroscience*, 28(10), 2539–2550.
- 701 Korzeniewska, A., Crainiceanu, C. M., Kus, R., Franaszczuk, P. J., & Crone, N. E. (2008). Dynamics
702 of event-related causality in brain electrical activity. *Human Brain Mapping*, 29(10).
- 703 Kumar, M., Anderson, M. J., Antony, J. W., Baldassano, C., Brooks, P. P., Cai, M. B., ... Norman,
704 K. A. (2021). BrainIAK: the brain image analysis kit. *Aperture*, doi.org/10.52294/31bb5b68-2184-
705 411b-8c00-a1dacb61e1da.
- 706 Laird, A. R., Fox, P. M., Eickhoff, S. B., Turner, J. A., Ray, K. L., McKay, D. R., ... Fox, P. T. (2011).
707 Behavioral interpretations of intrinsic connectivity networks. *Journal of Cognitive Neuroscience*,
708 23(12), 4022–4037.
- 709 Lerner, Y., Honey, C. J., Silbert, L. J., & Hasson, U. (2011). Topographic mapping of a hierarchy of
710 temporal receptive windows using a narrated story. *The Journal of Neuroscience*, 31(8), 2906–2915.
- 711 Lynn, C. W., & Bassett, D. S. (2021). Quantifying the compressibility of complex networks.
712 *Proceedings of the National Academy of Sciences, USA*, 118(32), e2023473118.
- 713 Mack, M. L., Preston, A. R., & Love, B. C. (2020). Ventromedial prefrontal cortex compressesion
714 during concept learning. *Nature Communications*, 11(46), doi.org/10.1038/s41467-019-13930-8.
- 715 Manning, J. R. (2023). Context reinstatement. In M. J. Kahana & A. D. Wagner (Eds.), *Handbook of
716 human memory*. Oxford University Press.
- 717 Manning, J. R., Zhu, X., Willke, T. L., Ranganath, R., Stachenfeld, K., Hasson, U., ... Norman,
718 K. A. (2018). A probabilistic approach to discovering dynamic full-brain functional connectivity
719 patterns. *NeuroImage*, 180, 243–252.
- 720 Norman, K. A., Polyn, S. M., Detre, G. J., & Haxby, J. V. (2006). Beyond mind-reading: multi-voxel
721 pattern analysis of fMRI data. *Trends in Cognitive Sciences*, 10(9), 424–430.
- 722 OpenAI. (2023). *ChatGPT*. <https://chat.openai.com>.

- 723 Owen, L. L. W., Chang, T. H., & Manning, J. R. (2021). High-level cognition during story listening is
724 reflected in high-order dynamic correlations in neural activity patterns. *Nature Communications*,
725 12(5728), doi.org/10.1038/s41467-021-25876-x.
- 726 Owen, L. L. W., Muntianu, T. A., Heusser, A. C., Daly, P., Scangos, K. W., & Manning, J. R. (2020). A
727 Gaussian process model of human electrocorticographic data. *Cerebral Cortex*, 30(10), 5333–5345.
- 728 Pelli, D. G. (1997). The VideoToolbox software for visual psychophysics: transforming numbers
729 into movies. *Spatial Vision*, 10, 437–442.
- 730 Preti, M. G., Bolton, T. A. W., & Van De Ville, D. (2017). The dynamic functional connectome:
731 state-of-the-art and perspectives. *NeuroImage*, 160, 41–54.
- 732 Regev, M., Simony, E., Lee, K., Tan, K. M., Chen, J., & Hasson, U. (2018). Propagation of information
733 along the cortical hierarchy as a function of attention while reading and listening to stories.
734 *Cerebral Cortex*.
- 735 Rogers, B. P., Morgan, V. L., Newton, A. T., & Gore, J. C. (2007). Assessing functional connectivity
736 in the human brain by fMRI. *Magnetic Resonance Imaging*, 25(11), 1347–1357.
- 737 Rubin, T. N., Kyoejo, O., Gorgolewski, K. J., Jones, M. N., Poldrack, R. A., & Yarkoni, T. (2017).
738 Decoding brain activity using a large-scale probabilistic functional-anatomical atlas of human
739 cognition. *PLoS Computational Biology*, 13(10), e1005649.
- 740 Rubinov, M., & Sporns, O. (2010). Complex network measures of brain connectivity: uses and
741 interpretations. *NeuroImage*, 52, 1059–1069.
- 742 Scangos, K. W., Khambhati, A. N., Daly, P. M., Owen, L. L. W., Manning, J. R., Ambrose, J. B.,
743 ... Chang, E. F. (2021). Biomarkers of depression symptoms defined by direct intracranial
744 neurophysiology. *Frontiers in Human Neuroscience*, 15, doi.org/10.3389/fnhum.2021.746499.
- 745 Schaefer, A., Kong, R., Gordon, E. M., Laumann, T. O., Z, X.-N., Holmes, A. J., ... Yeo, B. T. T. (2018).
746 Local-global parcellation of the human cerebral cortex from intrinsic functional connectivity MRI.
747 *Cerebral Cortex*, 28, 3095–3114.

- 748 Shannon, C. E. (1948). A mathematical theory of communication. *Bell System Technical Journal*,
749 27(3), 379–423.
- 750 Simony, E., & Chang, C. (2020). Analysis of stimulus-induced brain dynamics during naturalistic
751 paradigms. *NeuroImage*, 216, 116461.
- 752 Simony, E., Honey, C. J., Chen, J., & Hasson, U. (2016). Dynamic reconfiguration of the default
753 mode network during narrative comprehension. *Nature Communications*, 7(12141), 1–13.
- 754 Sizemore, A. E., Giusti, C., Kahn, A., Vettel, J. M., Betzel, R. F., & Bassett, D. S. (2018). Cliques and
755 cavities in the human connectome. *Journal of Computational Neuroscience*, 44(1), 115–145.
- 756 Smith, S. M., Beckmann, C. F., Andersson, J., Auerbach, E. J., Bijsterbosch, J., Douaud, G., ...
757 Glasser, M. F. (2013). Resting-state fMRI in the Human Connectome Project. *NeuroImage*, 80,
758 144–168.
- 759 Smith, S. M., Fox, P. T., Miller, K. L., Glahn, D. C., Fox, P. M., Mackay, C. E., ... Beckmann,
760 C. F. (2009). Correspondence of the brain's functional architecture during activation and rest.
761 *Proceedings of the National Academy of Sciences, USA*, 106(31), 13040–13045.
- 762 Smith, S. M., Hyvärinen, A., Varoquaux, G., Miller, K. L., & Beckmann, C. F. (2014). Group-PCA
763 for very large fMRI datasets. *NeuroImage*, 101, 738–749.
- 764 Smith, S. M., Vidaurre, D., Beckmann, C. F., Glasser, M. F., Jenkinson, M., Miller, K. L., ... Van
765 Essen, D. C. (2013). Functional connectomics from resting-state fMRI. *Trends in Cognitive Sciences*,
766 17(12), 666–682.
- 767 Sporns, O., & Betzel, R. F. (2016). Modular brain networks. *Annual Review of Psychology*, 67,
768 613–640.
- 769 Sporns, O., & Honey, C. J. (2006). Small worlds inside big brains. *Proceedings of the National Academy
770 of Sciences, USA*, 103(51), 19219–19220.
- 771 Sporns, O., & Zwi, J. D. (2004). The small world of the cerebral cortex. *Neuroinformatics*, 2(2),
772 145–162.

- 773 Srinivasan, R., Winter, W. R., Ding, J., & Nunez, P. L. (2007). EEG and MEG coherence: Measures of
774 functional connectivity at distinct spatial scales of neocortical dynamics. *Journal of Neuroscience*
775 *Methods*, 166, 41–52.
- 776 Sul, S., Güroğlu, B., Crone, E. A., & Chang, L. J. (2017). Medial prefrontal cortical thinning
777 mediates shifts in other-regarding preferences during adolescence. *Scientific Reports*, 7(8510),
778 doi.org/10.1038/s41598-017-08692-6.
- 779 Tomasi, D., & Volkow, N. D. (2011). Association between functional connectivity hubs and brain
780 networks. *Cerebral Cortex*, 21, 2003–2013.
- 781 Yeo, B. T. T., Krienen, F. M., Sepulcre, J., Sabuncu, M. R., Lashkari, D., Hollinshead, M., . . . Buckner,
782 R. L. (2011). The organization of the human cerebral cortex estimated by intrinsic functional
783 connectivity. *Journal of Neurophysiology*, 106(3), 1125–1165.